Applied Catalysis B: Environmental 136–137 (2013) 218–224

Contents lists available at SciVerse ScienceDirect

Applied Catalysis B: Environmental

journal homepage: www.elsevier.com/locate/apcatb

A ferromagnetic γ-alumina-supported iron catalyst for CWPO. Application to chlorophenols

Macarena Munoz [a,*], Zahara M. de Pedro [a], Nieves Menendez [b], Jose A. Casas [a], Juan J. Rodriguez [a]

[a] Seccion Departamental Ingenieria Quimica, Universidad Autonoma de Madrid, Crta. Colmenar km 15, 28049 Madrid, Spain
[b] Departamento de Quimica-Fisica Aplicada, Universidad Autonoma de Madrid, Crta. Colmenar km 15, 28049 Madrid, Spain

ARTICLE INFO

Article history:
Received 10 December 2012
Received in revised form 25 January 2013
Accepted 1 February 2013
Available online 10 February 2013

Keywords:
Heterogeneous Fenton
Ferromagnetic catalyst
Chlorophenol

ABSTRACT

A ferromagnetic γ-Al_2O_3-supported iron catalyst has been prepared and its activity and stability in catalytic wet peroxide oxidation (CWPO) have been compared with those of a previous iron-based conventional catalyst using the same support. Both catalysts were characterized by nitrogen adsorption–desorption isotherms, ICP, TXRF, XRD, XPS, elemental analysis and Mössbauer spectroscopy. The behavior of these catalysts in CWPO of chlorophenols has been related with the nature of the dominant iron species (magnetite or hematite). The results showed that the magnetic catalyst improved significantly the decomposition of H_2O_2 leading to an increased degradation and mineralization of chlorophenols. Complete conversion of those target pollutants and more than 75% TOC reduction were achieved after 4 h under stoichiometric H_2O_2 dose, 100 mg L^{-1} initial chlorophenol concentration, 1 g L^{-1} catalyst, pH 3 and 50 °C temperature. Moreover, complete dechlorination of all the chlorophenols tested was achieved, being the residual organic by-products short-chain acids without significance in terms of ecotoxicity. The catalyst showed a remarkable stability in long-term continuous experiments with limited Fe leaching, below 5% of the initial loading after 100 h on stream. An additional clear advantage of the new catalyst is its easy separation and recovery from the reaction medium by applying an external magnetic field.

1. Introduction

Chlorophenols (CPs) are pollutants commonly found in a wide variety of industrial wastewaters since they are used in the manufacture of a diversity of chemical products, like pesticides, herbicides, germicides, fungicides and wood preservatives. These waste streams pose important pollution problems associated to the high toxicity of chlorophenols, which have been listed as priority pollutants by the European Decision 2455/2001/EC [1]. The development of efficient technologies for those industrial wastewaters has focused considerable research efforts in the last years. Advanced oxidation processes (AOPs) have been claimed as potential solution in that respect [2] and in particular the Fenton process has gained a major attention due to its simplicity of design, implementation and operation (near ambient conditions) and its ability to deal with a wide diversity of pollutants [3–5]. Nevertheless, an important drawback of the conventional Fenton is that the catalyst, iron in solution, cannot be retained in the process, requiring further separation to prevent additional water pollution. In this sense, the use of solid catalysts by immobilization of the active iron over a convenient support offers a practical solution. Research within the last decade has proved that hydrogen peroxide can oxidize organic pollutants in the presence of Fe-bearing solid catalysts in the so-called catalytic wet peroxide oxidation (CWPO). Important efforts have been focused on finding catalysts with adequate activity and stability, taking into account the acidic conditions at which the reaction takes place. So far, mesostructured materials [6–8], zeolites [9,10], pillared clays [11–14] and activated carbon [15,16] have been used as supports to prepare these catalysts. Unfortunately, most of them showed relatively low activities or strong iron leaching due to the acidic pH or the low chemical stability of the supports [16,17]. Recently, iron supported on γ-Al_2O_3 (Fe/γ-Al_2O_3) has proved to be an excellent highly-stable catalyst for CWPO not only with aqueous phenol but with real wastewaters from the cosmetic industry [18,19].

Usually, CWPO catalysts have been used in powdered form (d_p < 100 μm), making difficult its separation and recovery from solution. In this sense, ferromagnetic catalysts are receiving increasing attention since they can be easily separated from the liquid phase by applying a magnetic field. Recent studies have been focused on magnetite as catalyst for heterogeneous Fenton oxidation [20,21]. Nonetheless, so far only few papers have been issued

* Corresponding author. Tel.: +34 91 497 3991; fax: +34 91 497 3516.
E-mail address: macarena.munnoz@uam.es (M. Munoz).

0926-3373/$ – see front matter © 2013 Elsevier B.V. All rights reserved.
http://dx.doi.org/10.1016/j.apcatb.2013.02.002

on the synthesis of mesoporous materials containing ferromagnetic nanoparticles [21–24]. To incorporate magnetic nanoparticles in mesoporous materials, post-synthetic impregnation methods have been generally employed, which require multiple and complicated steps. The post-synthetic incorporation of magnetic nanoparticles in porous hosts could also block the main pores of mesoporous materials [25]. In this sense, a short and simple synthetic procedure should be developed looking for practical application of magnetic catalysts.

In this work, a ferromagnetic and a conventional non-magnetic iron-on-γ-alumina catalyst have been prepared and tested in the CWPO of chlorophenols in aqueous solution at atmospheric pressure and at 50 °C. The activity and stability of the catalysts have been analyzed in relation with the dominant iron species. The effect of the chlorine content of chlorophenols was also studied by using 4-chlorophenol (4-CP), 2,4-dichlorophenol (2,4-DCP) and 2,4,6-trichlorophenol (2,4,6-TCP) as target compounds. The results obtained have been analyzed in terms of hydrogen peroxide decomposition, chlorophenol conversion, overall dechlorination and TOC reduction. The stability of the catalyst was assessed by long-term continuous experiments.

2. Materials and methods

2.1. Catalysts preparation and characterization

The catalysts were prepared by incipient wetness impregnation of powdered γ-Al_2O_3 (d_p < 100 μm) supplied by Merck (Germany) with a $Fe(NO_3)_3{\cdot}9H_2O$ aqueous solution. The Fe load was adjusted to a nominal 4% (w/w). After impregnation, the solids were left for 2 h at room temperature, dried for 12 h at 60 °C and calcined for 4 h at 300 °C. An additional reduction stage in H_2 atmosphere was carried out for 2 h at 350 °C in order to develop magnetic properties in one of the catalysts. Thus, the identification of the catalysts was Fe_2O_3/γ-Al_2O_3 and Fe_3O_4/γ-Al_2O_3 for the non-magnetic and the magnetic catalyst, respectively.

The porous structure of the fresh and used catalysts was characterized from nitrogen adsorption–desorption isotherms at −196 °C using a Micromeritics Tristar 3020 apparatus. The samples were previously outgassed overnight at 150 °C to a residual pressure of 10^{-3} Torr. Total iron content was analyzed by inductively coupled plasma (ICP/MS) with a ICP-MS Elan 6000 PerkinElmer Sciex. Elemental analyses of the fresh and used catalysts were carried out in a LECO CHNS-932 Elemental Analyzer. The chlorine content of the used catalysts was determined by total reflection X-ray fluorescence (TXRF), using a TXRF spectrometer 8030c. The iron particles of the Fe_xO_y/γ-Al_2O_3 were characterized by transmission electron microscopy (TEM) at 400 kV (JEOL, mod. JEM-4000 EX). Software "ImageJ 1.44i" was used for counting and measuring particles on digital TEM images (more than 200 nanoparticles were measured per image). The crystalline phases in the catalysts were analyzed by X-ray diffraction (XRD) using a Siemens model D-5000 diffractometer with Cu Kα radiation. The iron species in the fresh and used catalysts were also identified by Mössbauer spectroscopy. Mössbauer spectra at room temperature and 77 K were recorded in triangle mode using a conventional spectrometer with ^{57}Co(Rh) source. The spectra were analyzed by a non-linear fit using the NORMOS program [26] and the energy calibration was made using a α-Fe (6 μm) foil. X-ray photoelectron spectroscopy (XPS) was employed for surface iron analysis using a Physical Electronics, model ESCA 5701 apparatus equipped with a Mg-Kα X-ray excitation source, 1253.6 eV. Software "Multipak v8.2b" was used for spectrograms deconvolution in order to determine both Fe (II) and Fe (III) species on the surface of the catalysts. Magnetic measurements were performed using a Quantum Design MPMS XL-5 superconducting quantum interference device (SQUID). The magnetic moment M was measured as function of applied magnetic field H at room temperature.

2.2. CWPO experiments

CWPO runs were carried out at atmospheric pressure and at 50 °C. All of the experiments in this work were performed in a glass batch reactor (450 mL) equipped with a PTFE stirrer (700 rpm) and a temperature control. The aforementioned temperature has been reported as the optimum for this process [19,27,28], because of the enhanced efficiency of H_2O_2 consumption. Increasing the temperature above the ambient has demonstrated a beneficial effect on that respect which is crucial in the economy of the process [29]. The initial pH of the reaction medium was adjusted with nitric acid to the optimum value (pH 3) in all the experiments [18]. A starting chlorophenol concentration of 100 mg L^{-1} was always used which can be considered a representative concentration of chlorophenols in industrial wastewaters [30–32]. According to previous works [19,33,34], the theoretical stoichiometric amount of H_2O_2 for complete oxidation of each chlorophenol to CO_2, H_2O and HCl, and 1 g L^{-1} of powdered Fe_xO_y/γ-Al_2O_3 catalyst (d_p < 100 μm) were used in all the experiments.

Long-term experiments were carried out in a 500 mL glass continuous stirred (700 rpm) tank reactor at 2 mL min^{-1} flow rate over 100 h using 500 mg of catalyst, 50 °C and initial pH 3. In order to avoid the loss of catalyst from the reactor a Swagelok filter was placed at the exit. The starting 2,4,6-TCP and H_2O_2 concentrations were 100 and 190 mg L^{-1}, respectively.

In each run, samples were periodically withdrawn in order to follow the progress of the reaction. Chlorophenols and the main aromatic by-products were quantified by means of high-performance liquid chromatography (HPLC; Varian Pro-Start 325) using a UV detector and a Microsorb C18 5 μm column (MV 100, 15 cm length, 4.6 mm diameter) as the stationary phase. The analyses were carried out at 270 nm using a 70/30, 55/45 and 45/55% (v/v) mixture of acetonitrile/acetic acid aqueous solution (75 mM) as the mobile phase for 4-CP, 2,4-DCP and 2,4,6-TCP, respectively. Short-chain acids and chloride ion were analyzed by ion chromatography with chemical suppression (Metrohm 790 IC) using a conductivity detector. A Metrosep A supp 5-250 column (25 cm length, 4 mm internal diameter) was used as stationary phase and a 3.2 mM Na_2CO_3 aqueous solution as the mobile phase. Total organic carbon (TOC) was measured using a TOC analyzer (Shimadzu, mod. TOC, VSCH) and the H_2O_2 concentration was determined by colorimetric titration using the titanium sulfate method [35] with an UV 1603 Shimazdu UV/Vis spectrophotometer. Fe leached from the catalyst to the reaction medium was measured according to the o-phenantroline method [36].

To evaluate the ecotoxicity of the reaction effluents, a standard method (Microtox M500 Analyzer) was used. The Microtox test (ISO 11348-3, 1998) is based on measuring the intensity of the bioluminescence emitted by the marine bacteria *Vibrio fischeri*. The bioluminescence was measured in a M500 Microtox Analyzer (Azur Environmental). The test was carried out at 15 °C, adjusting the osmotic pressure close to 2% NaCl and pH between 6 and 8. The EC_{50} is defined as the effective nominal concentration (mg L^{-1}) of the target compound that reduces the intensity of light emission by 50% after 15 min contact time. For complex samples, IC_{50} is used, defined as the dilution ratio (%) of the sample that yields this 50% light emission reduction. The IC_{50} values are inversely proportional to the biological toxicity expressed as toxicity units (TU).

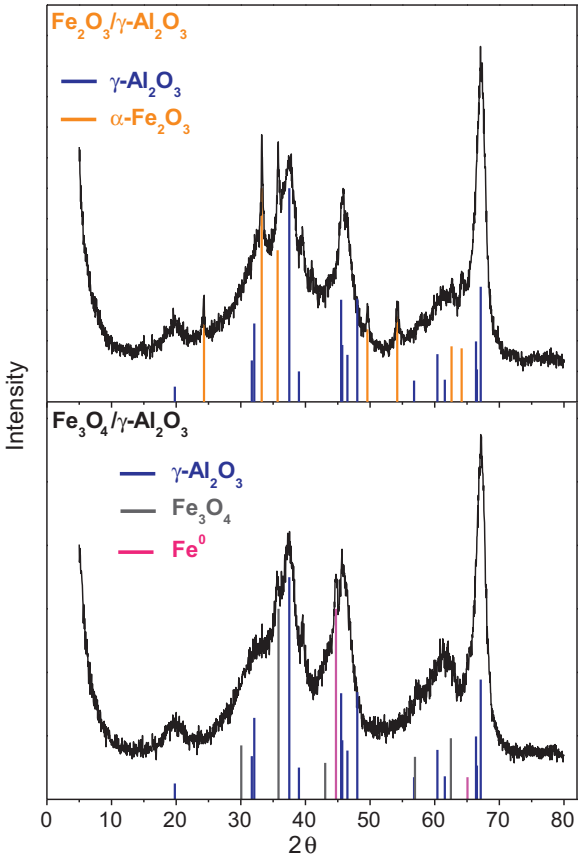

Fig. 1. XRD patterns of the Fe_2O_3/γ-Al_2O_3 and Fe_3O_4/γ-Al_2O_3 catalysts. Major peaks are identified using ICDD PDF 04-008-4096 (γ-Al_2O_3), PDF 04-008-7623 (α-Fe_2O_3), PDF 04-004-6370 (Fe^0) and PDF 04-011-5952 (Fe_3O_4).

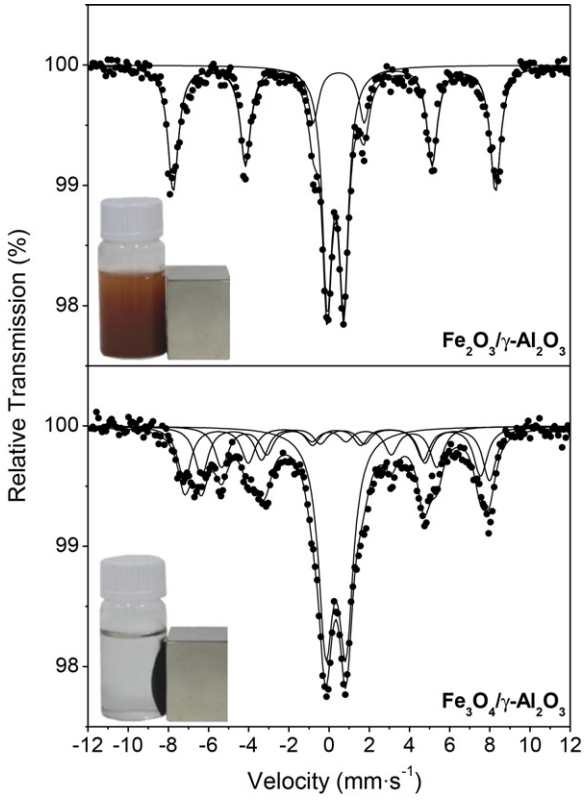

Fig. 2. Room temperature Mössbauer spectra of the Fe_2O_3/γ-Al_2O_3 and Fe_3O_4/γ-Al_2O_3 catalysts, and the photographs of the samples under a magnetic field.

3. Results and discussion

3.1. Catalysts characterization

The characterization of the porous structure of the raw alumina and the two catalysts allows establishing the mesoporous character of the solids since the BET and external (namely non microporous) areas were almost coincident. Impregnation of the support led to a slight decrease of the BET surface area from 141 $m^2\,g^{-1}$ of the alumina to 136 $m^2\,g^{-1}$ of the Fe_2O_3/γ-Al_2O_3 catalyst. Reduction of the catalyst (Fe_3O_4/γ-Al_2O_3) did not produce any further change of the BET surface area. According to the ICP-MS analyses the Fe content of the fresh catalysts was close to the nominal 4% (w/w) (3.8% w/w for both Fe_2O_3/γ-Al_2O_3 and Fe_3O_4/γ-Al_2O_3). The catalysts were also characterized by transmission electron microscopy (TEM). The iron nanoparticles presented a wide range of sizes in the range of 5–45 nm, showing a mean diameter of 25 and 33 nm for Fe_2O_3/γ-Al_2O_3 and Fe_3O_4/γ-Al_2O_3 catalysts, respectively (see Fig. S1 in the Supplementary Material for size distribution of both catalysts).

XRD patterns of the catalysts are shown in Fig. 1. As can be seen, the profile of the Fe_2O_3/γ-Al_2O_3 catalyst showed two crystalline phases, corresponding to γ-Al_2O_3 and hematite (α-Fe_2O_3). The magnetic catalyst presented three crystalline phases now corresponding to γ-Al_2O_3, metallic iron (Fe^0) and magnetite (Fe_3O_4).

The presence of hematite and magnetite in the catalysts was also confirmed by Mössbauer spectroscopy. Mössbauer spectra (Fig. 2) were collected at room temperature. As can be seen, the Fe_2O_3/γ-Al_2O_3 catalyst presented a central doublet and a hyperfine magnetic field distribution (sextet). The average distribution field (H = 49.7 T) is typical of small hematite (α-Fe_2O_3) particles lower than bulk [37], showing a typical field value of 51.5 T [38]. The spectrum of the magnetic catalyst contained three sextets, with a magnetic hyperfine field value of 47.0 and 43.0 T, corresponding to Fe (III) in the tetrahedral positions and Fe (II)/Fe (III) in the octahedral positions of the magnetite, respectively. These values are typical of small particles, lower than bulk, which present a field value of 49.1 T and 45.3 T for the tetrahedral and octahedral positions, respectively [38]. The third sextet, with magnetic field value of 33.2 T is identified as metallic iron, formed also in the reduction process. The relative concentration of this species was below 10%. In both catalysts the central doublet can be identified as iron oxide nanoparticles, Fe_2O_3 or Fe_3O_4, smaller than 10 nm and therefore superparamagnetics.

The catalysts were also characterized by XPS. Fe 2p core level XPS spectra for both catalysts are shown in Fig. 3. The XPS spectrum of the Fe_3O_4/γ-Al_2O_3 catalyst shows two bands centered at binding energy values around 710.6 and 724.1 eV for Fe $2p_{3/2}$ and Fe $2p_{1/2}$, respectively, which can be attributed to Fe_3O_4 [39]. On the other hand, the XPS spectrum of the Fe_2O_3/γ-Al_2O_3 catalyst shows that those bands are slightly displaced at binding energy values around 711 and 724.6 eV for Fe $2p_{3/2}$ and Fe $2p_{1/2}$, respectively, corresponding to Fe_2O_3 [39]. A satellite band at 718.8 eV can be observed in the case of the Fe_2O_3/γ-Al_2O_3 catalyst. The absence of this satellite band is also a common feature of the magnetite XPS spectrum. The presence of metallic iron was not clearly distinguishable in the XPS spectrum of the magnetic catalyst since the two bands were not displaced to binding energies of 706.7 and 719.8, which are the specific ones for metallic iron [40]. This fact can be directly attributed to the low concentration of metallic iron present in the catalyst. Deconvolution of the core level spectra of Fe 3p orbitals for both Fe_2O_3/γ-Al_2O_3 and Fe_3O_4/γ-Al_2O_3 catalysts are depicted in Fig. 4. According to Yamashita and Hayes [39], for the Fe 3p core

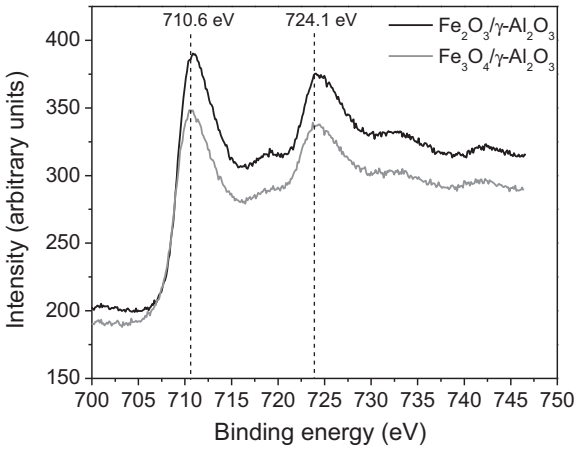

Fig. 3. Fe 2p core level XPS spectra of Fe_2O_3/γ-Al_2O_3 and Fe_3O_4/γ-Al_2O_3 catalysts.

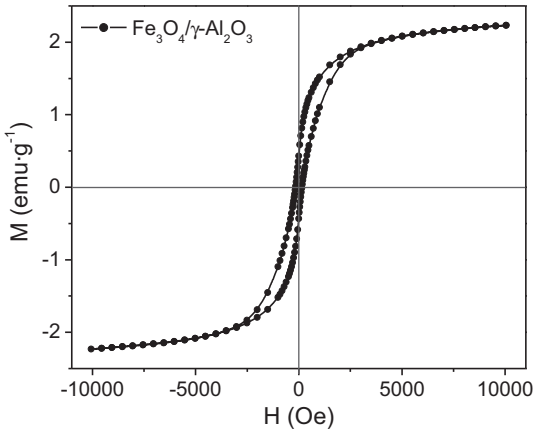

Fig. 5. Magnetization hysteresis loop of Fe_3O_4/γ-Al_2O_3 catalyst.

level, the bands corresponding to Fe (III) and Fe (II) are centered at binding energy values around 55.6 and 53.8 eV, respectively. Thus, from Fig. 4 the only presence of Fe (III) in the Fe_2O_3/γ-Al_2O_3 catalyst can be confirmed. On the other hand, the relative proportions of Fe (II) and Fe (III) were calculated for the Fe_3O_4/γ-Al_2O_3 catalyst upon integration of the areas under the curves, obtaining a Fe (II): Fe (III) ratio of 0.30:0.70, which is close to the theoretical stoichiometric ratio of magnetite (0.33:0.67) [39].

Fig. 5 illustrates the magnetization curve of the Fe_3O_4/γ-Al_2O_3 catalyst. The saturation magnetization value (M_S) was found to be 2.24 emu g^{-1}, fairly higher than those reported by other authors [41,42]. Taking into account the M_S value of bulk magnetite (92 emu g^{-1}), the value of saturation magnetization expected if all the iron in the catalyst (3.8 wt.%) was as magnetite would be 3.49 emu g^{-1}. The M_S specific value for the Fe_3O_4/γ-Al_2O_3 catalyst is slightly lower than this value, which can be due to the smaller particle size and the surface-related effects such as surface disorder [21].

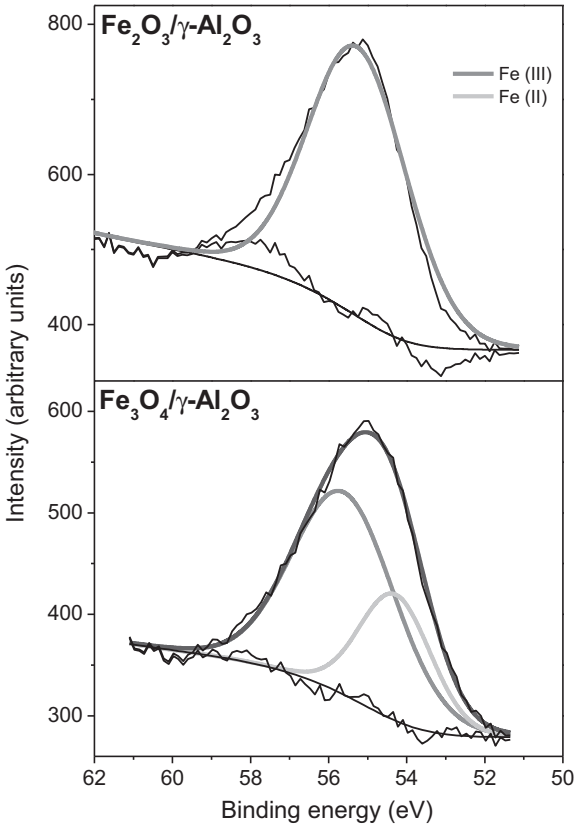

Fig. 4. Deconvolution of the core level spectra of Fe 3p orbitals of Fe_2O_3/γ-Al_2O_3 and Fe_3O_4/γ-Al_2O_3 catalysts.

3.2. Catalytic activity

3.2.1. H_2O_2 decomposition

In a first approach to assess the activity of the catalysts, their ability to decompose H_2O_2 was analyzed (Fig. 6). Although both catalysts are capable of decomposing H_2O_2, significant differences were observed in the reaction rate. The values obtained for the pseudo-first order rate constant with Fe_2O_3/γ-Al_2O_3 and Fe_3O_4/γ-Al_2O_3 were 2.4×10^{-3} and 7.3×10^{-3} min^{-1}, respectively. Thus, the Fe_3O_4/γ-Al_2O_3 catalyst decomposes H_2O_2 about three times faster than the Fe_2O_3/γ-Al_2O_3 one. This can be related with the presence of both Fe (II) and Fe (III) in the Fe_3O_4/γ-Al_2O_3 catalyst which enhances the decomposition of H_2O_2. Iron leaching from both catalysts under these operating conditions was negligible (<0.1 mg L^{-1}) and thus, H_2O_2 decomposition by homogeneous Fenton reaction can be discarded.

3.2.2. Chlorophenols oxidation

Fig. 7 shows the evolution of the three chlorophenols tested (4-CP, 2,4-DCP and 2,4,6-TCP) and H_2O_2 in the oxidation runs performed with the two catalysts investigated. Both catalysts showed

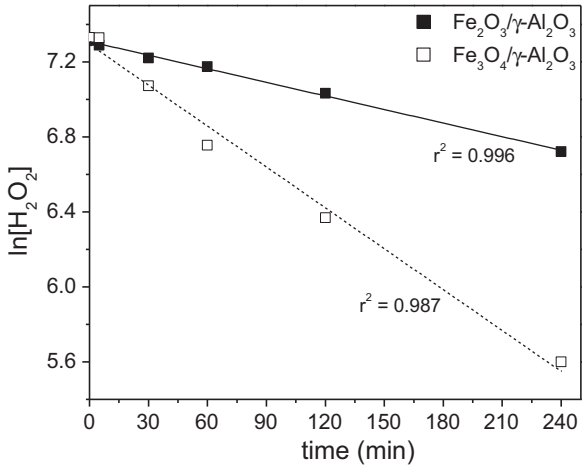

Fig. 6. H_2O_2 decomposition with the Fe_2O_3/γ-Al_2O_3 and Fe_3O_4/γ-Al_2O_3 catalysts. ($[Fe_xO_y/\gamma$-$Al_2O_3] = 2$ g L^{-1}; $[H_2O_2]_0 = 1500$ mg L^{-1}; $pH_0 = 3$; $T = 50$ °C).

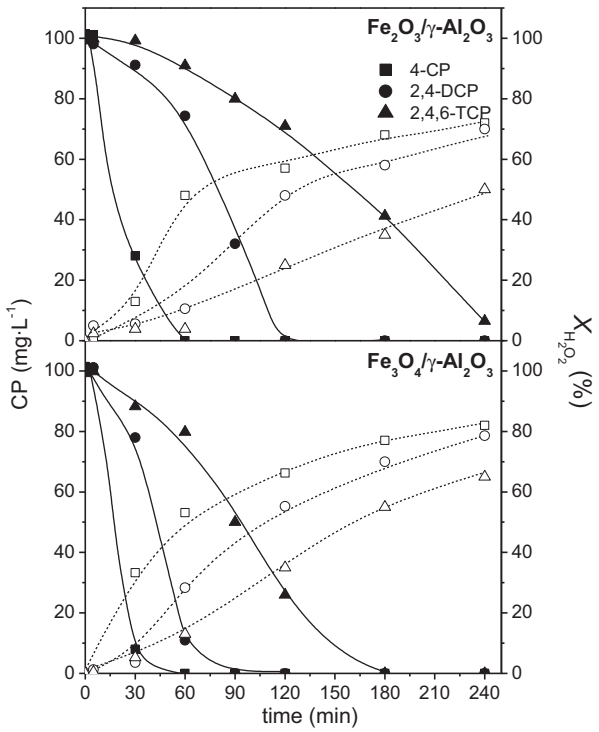

Fig. 7. Evolution of 4-CP, 2,4-DCP and 2,4,6-TCP concentration (solid symbols) and H_2O_2 conversion (open symbols) upon CWPO with Fe_xO_y/γ-Al_2O_3 catalysts ($[CP]_0 = 100\,mg\,L^{-1}$; $[Fe_xO_y/\gamma\text{-}Al_2O_3] = 1\,g\,L^{-1}$; $[H_2O_2]_0$ = stoichiometric dose; $pH_0 = 3$; $T = 50\,^{\circ}C$).

an efficient use of H_2O_2 whose decomposition must be occurring mainly through the formation of $^{\bullet}OH$ radicals since the conversion of H_2O_2 was associated to a significant reduction of chlorophenols concentration. As can be seen, the magnetic catalyst promoted a faster degradation of the three chlorophenols consistent with a faster decomposition of H_2O_2 in all the cases. As explained above, the higher activity of the magnetic catalyst can be related with the presence of Fe (II) in addition to Fe (III) being this last the only iron species in the non-magnetic catalyst.

The chlorine content of each target chlorophenol showed a significant effect on the rate of oxidation (Fig. 7). Chlorine could be blocking some favorable positions of the aromatic ring susceptible to hydroxyl radical attack, thus inhibiting oxidation. Consequently, the oxidation rate decreases according to the following order: 4-CP > 2,4-DCP > 2,4,6-TCP. Tang and Huang [43] reported similar conclusions on the effect of the chlorine content of chlorophenols in homogeneous Fenton oxidation. They found a linear correlation between the rate constants and the number of sites available in the molecule and explained their conclusion on the basis of steric hindrance.

A pseudo-first order kinetic model was used to fit the time-evolution of H_2O_2 upon CWPO of 4-CP, 2,4-DCP and 2,4,6-TCP. Table 1 reports the values of the pseudo-first order rate constants for hydrogen peroxide decomposition with the two catalysts tested. As can be observed, both the type of iron species in the catalyst and the chlorine content of the target chlorophenol affected significantly to the rate of H_2O_2 decomposition, whose trend is consistent with that of chlorophenols degradation.

Fig. 8 presents again the evolution of chlorophenols but now in a mole basis together with that of chloride ion for the sake of easily following the dechlorination process. The results demonstrate that dechlorination of chlorophenols upon CWPO is highly effective since the chloride concentration at the end of the 4 h experiments was coincident with the initial chlorine content

Table 1
Pseudo-first order rate constant values for H_2O_2 decomposition upon CWPO of 4-CP, 2,4-DCP and 2,4,6-TCP with Fe_xO_y/γ-Al_2O_3 catalysts ($[CP]_0 = 100\,mg\,L^{-1}$; $[Fe_xO_y/\gamma\text{-}Al_2O_3] = 1\,g\,L^{-1}$; $[H_2O_2]_0$ = stoichiometric dose; $pH_0 = 3$; $T = 50\,^{\circ}C$).

Catalyst	Chlorophenol	k (10^3 min^{-1})	r^2
Fe_2O_3/γ-Al_2O_3	4-CP	4.46	0.947
	2,4-DCP	4.24	0.969
	2,4,6-TCP	1.98	0.956
Fe_3O_4/γ-Al_2O_3	4-CP	8.31	0.976
	2,4-DCP	6.12	0.994
	2,4,6-TCP	3.65	0.981

of each chlorophenol. However, the dechlorination is slightly slower than chlorophenol conversion in the initial stages of reaction indicating that chlorinated intermediates are formed along the oxidation process which finally evolve to non-chlorinated by-products. According to the literature [33,34,44,45], the first by-products obtained in the oxidation of chlorophenols are chlorobenzenediols formed by hydroxylation of the aromatic ring. However, in this work no chlorobenzenediols were detected probably because they appeared only in trace amounts.

Fairly high mineralization percentages (≈75%) were achieved at the end of the experiments (4 h) upon CWPO of all the chlorophenols tested using the two catalysts. Considering that the H_2O_2 consumed in the reactions was about 80%, the efficiency of H_2O_2 was calculated as 90% in our system for the oxidation of the three chlorophenols studied with both catalysts. The magnetic catalyst led to higher mineralization rates with all the chlorophenols tested although at the end of the 4 h-experiments the mineralization percentage was only slightly higher than with the non-mangnetic catalyst (see Fig. S2 of Supplementary Material). The two

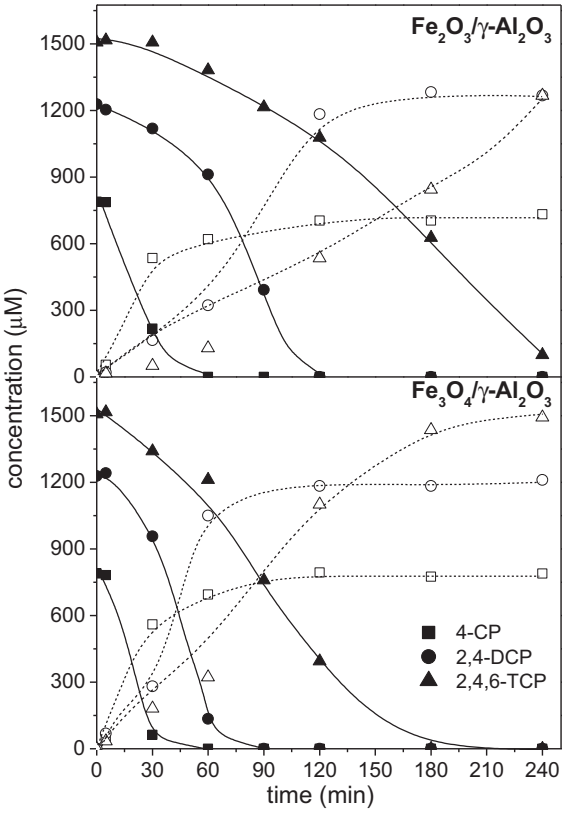

Fig. 8. Evolution of 4-CP, 2,4-DCP and 2,4,6-TCP (solid symbols) and chloride ion (open symbols) concentration upon CWPO with Fe_xO_y/γ-Al_2O_3 catalysts ($[CP]_0 = 100\,mg\,L^{-1}$; $[Fe_xO_y/\gamma\text{-}Al_2O_3] = 1\,g\,L^{-1}$; $[H_2O_2]_0$ = stoichiometric dose; $pH_0 = 3$; $T = 50\,^{\circ}C$).

catalysts, specially the magnetic one, clearly improved the efficiency of H_2O_2 consumption with respect to the homogeneous Fenton [34] as well as compared with other CWPO catalysts [16], including the recently reported magnetic nanoparticles [21]. Those efficiencies rarely exceeded 75%.

The oxidation by-products remaining after the 4 h reaction time of the experiments consisted only in short-chain organic acids without significance in terms of toxicity since aromatic intermediates were not detected under these operating conditions. In fact, the ecotoxicity of the CWPO effluents was measured by the Microtox toxicity test confirming the non-toxic character of these streams (see Table S1 in Supplementary Material). The evolution of organic acids can be seen in Figs. S3–S5 of Supplementary Material. Fumaric, maleic, malonic, acetic, oxalic and formic acids were the main oxidation by-products identified. Chloroacetic acid was also found but its concentration was always below 3 mg L^{-1}. Oxalic deserves a particular attention since its concentration increased progressively in the reaction medium, showing a refractory behavior to CWPO, in agreement with the findings of other authors [3,16]. This acid has been demonstrated to provoke a negative effect on the stability of supported Fe catalysts due to metal leaching [15].

The distribution of short-chain organic acids resulting from the oxidation of 4-CP, 2,4-DCP and 2,4,6-TCP showed similar trends. The only difference refers to the time-evolution of these by-products. With the magnetic catalyst the formation and degradation of the short-chain organic acids was slightly displaced to shorter reaction times.

The TOC values calculated from all the species identified in the reaction medium was close to 95% of the measured TOC at the end of the 4 h reaction time. As shown in Fig. 8, the chlorine balance at that reaction time was matched almost completely, being that element as chloride ion except very small amounts of chloroacetic acid.

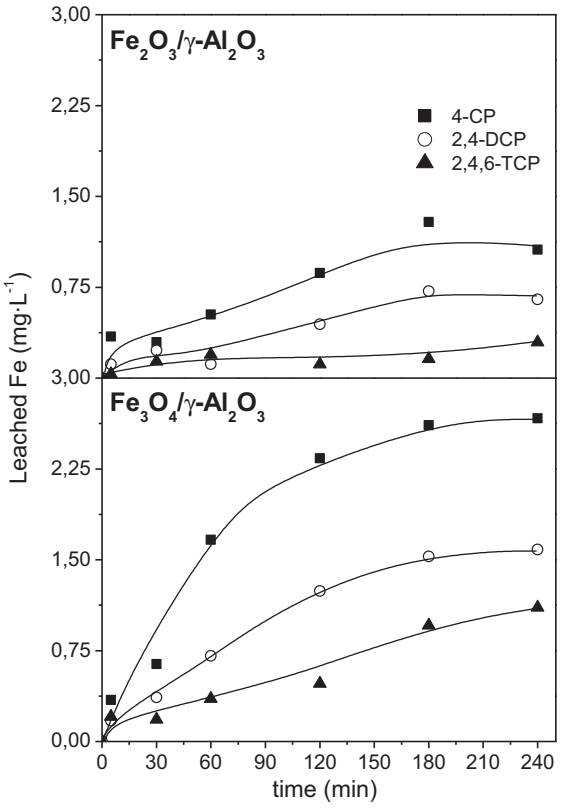

Fig. 9. Fe leaching from the Fe_xO_y/γ-Al_2O_3 catalysts upon CWPO of 4-CP, 2,4-DCP and 2,4,6-TCP ($[Fe_xO_y/\gamma\text{-}Al_2O_3] = 1$ g L^{-1}; $[H_2O_2]_0$ = stoichiometric dose; $pH_0 = 3$; $T = 50$ °C).

3.2.3. Stability of the catalysts

A relevant issue with regard to the potential application of these catalysts is the possible leaching of iron under the operating conditions. Fig. 9 shows the results obtained on that respect. The amount of Fe lost from the catalyst after used was somewhat higher in the case of the magnetic one, reaching around 6% of the initial iron load after 4 h reaction time in the experiments with 4-CP and being significantly lower with the two other chlorophenols tested. The increased iron leaching as the chlorine content of the starting chlorophenol decreases is in good agreement with the higher concentration of oxalic acid in the reaction medium (see Figs. S3–S5 of Supplementary Material). Anyway, iron leaching is substantially lower than the previously reported in the literature with other iron-catalyst for CWPO [15,16,21]. Xu and Wang [21] reported close to 10% iron leaching after 3 h of reaction in the CWPO of 2,4-DCP with magnetic nanoparticles under similar operating conditions.

The homogeneous contribution can be considered negligible since the release of iron was gradual and the maximum Fe concentration never exceeded 3 mg L^{-1}. At that point, H_2O_2 concentration was very small and the chlorophenol had been completely removed and highly mineralized. In fact, the degree of mineralization achieved with the Fe_xO_y/γ-Al_2O_3 catalysts was always significantly higher than that obtained by the homogeneous Fenton process (10 mg L^{-1} Fe^{3+}) under similar operating conditions [33,34].

The magnetic catalyst was easily and quickly separated from the reaction system by applying an external magnetic field after being used. In fact, the M_S values did not decrease more than 5% in the poorest conditions, i.e. in the oxidation of 4-CP which led to the highest leaching of iron ($M_S = 2.11$ emu g^{-1}). The magnetization curves of the used catalysts are included in the Fig. S6 of the Supplementary Material.

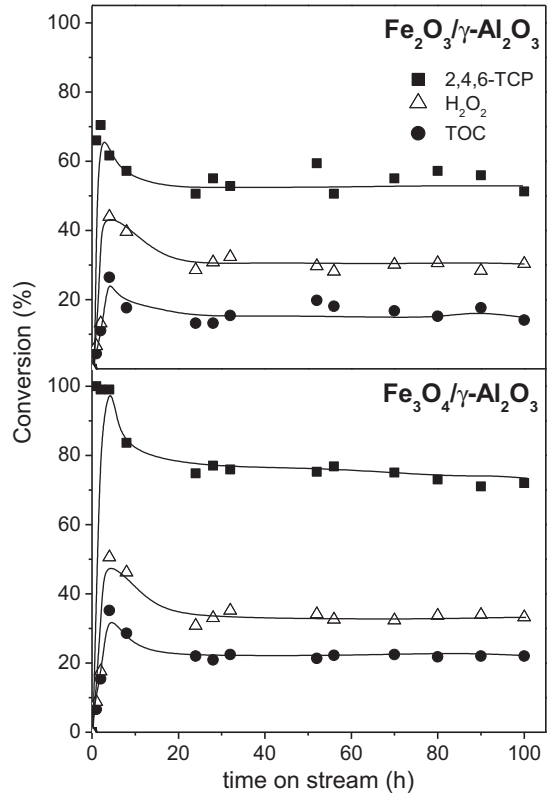

Fig. 10. Long-term performance of the Fe_xO_y/γ-Al_2O_3 catalysts upon CWPO of 2,4,6-TCP ($[Fe_xO_y/\gamma\text{-}Al_2O_3] = 1$ g L^{-1}; $[H_2O_2]_0$ = stoichiometric dose; $pH_0 = 3$; $T = 50$ °C; $\tau = 16.5$ kg_{cat} h mol^{-1}).

The Mössbauer spectra of the used catalysts did not show any significant change and neither did the XRD profiles (see Figs. S7 and S8 of Supplementary Material for the Mössbauer and XRD spectra). However it appeared a new XRD peak around 18° which can be attributed to the deposition of carbon-containing matter on the catalyst surface. This has been also reported by Bautista et al. [18] for a γ-alumina-supported Fe catalyst used in the CWPO of cosmetic wastewater. These authors observed that the deposits disappeared upon calcination at 550 °C without significant reduction of the catalytic activity.

To address the stability of the catalysts, long-term (100 h on stream) experiments were carried out in a continuous stirred tank reactor at 50 °C. A 100 mg L^{-1} 2,4,6-TCP and 190 mg L^{-1} H_2O_2 aqueous solution at pH 3 was fed at a 2 mL min^{-1} flow rate. The catalyst concentration was 1 g L^{-1}. The results are shown in Fig. 10. As can be seen, both catalysts showed a high stability since H_2O_2, 2,4,6-TCP and TOC conversions were maintained almost constant over the 100 h on stream (Fig. 10). Analysis by ICP-MS revealed that the loss of iron from the catalysts was around 5% of the initial load after the 100 h on stream. The BET surface area remained also unchanged. The catalysts were further analyzed by TXRF and elemental chemical analysis in order to gain information about possible chlorinated carbonaceous deposits on their surface. Small amounts of residual carbon-containing species (≈1.2% w/w) were measured.

4. Conclusions

A ferromagnetic catalyst has been prepared by a simple procedure consisting in impregnating γ-alumina with ferric nitrate followed by calcination at 300 °C and reduction under H_2 flow at 350 °C. The catalyst showed ferromagnetic properties allowing easy separation from the liquid phase. Its activity was investigated in the CWPO of mono-, di- and tri-chlorophenol. The catalyst allowed achieving complete conversion of chlorophenol and dechlorination with 75% mineralization after 4 h reaction time at 50 °C and pH 3 using the stoichiometric dose of H_2O_2. Fairly low iron leaching (<5%) and a high stability were demonstrated upon 100 h on stream. This new catalyst compared favorably with a previously used non-magnetic one also based in iron on γ-alumina.

Acknowledgments

This research has been supported by the Spanish MICINN through the projects CTQ2008-03988 and CTQ2010-14807 and by the CM through the project S-2009/AMB-1588. M. Munoz thanks the Spanish Ministry of Education for a FPU research grant.

Appendix A. Supplementary data

Supplementary data associated with this article can be found, in the online version, at http://dx.doi.org/10.1016/j.apcatb.2013.02.002.

References

[1] European Decision 2455/2001/EC of the European Parliament and the Council of 20 November 2001 establishing the list of priority substances in the field of water policy and amending Directive 2000/60/EC.
[2] M. Pera-Titus, V. García-Molina, M.A. Baños, J. Giménez, S. Esplugas, Applied Catalysis B 47 (2004) 219–256.
[3] J.A. Zazo, J.A. Casas, A.F. Mohedano, M.A. Gilarranz, J.J. Rodriguez, Environmental Science and Technology 39 (2005) 9295–9302.
[4] P. Bautista, A.F. Mohedano, M.A. Gilarranz, J.A. Casas, J.J. Rodriguez, Journal of Hazardous Materials 143 (2007) 128–134.
[5] M. Munoz, Z.M. de Pedro, J.A. Casas, J.J. Rodriguez, Chemical Engineering Journal 198–199 (2012) 275–281.
[6] C. Cooper, R. Burch, Water Research 33 (1999) 3689–3694.
[7] S. Chaliha, K.G. Bhattacharayya, Journal of Hazardous Materials 150 (2008) 728–736.
[8] P. Shukla, S. Wang, H. Sun, H.M. Ang, M. Tadé, Chemical Engineering Journal 164 (2010) 255–260.
[9] D.J. Doocey, P.N. Sharrat, Process Safety and Environment Protection 82 (2004) 352–358.
[10] E.V. Kuznetsova, E.N. Savinov, L.A. Vostrikova, V.N. Parmon, Applied Catalysis B 51 (2004) 165–170.
[11] J.G. Carriazo, M.A. Centeno, J.A. Odriozola, S. Moreno, R. Molina, Applied Catalysis A 317 (2007) 120–128.
[12] M. Luo, D. Bowden, P. Brimblecombe, Applied Catalysis B 85 (2009) 201–206.
[13] C.B. Molina, A.H. Pizarro, V.M. Monsalvo, A.M. Polo, A.F. Mohedano, J.J. Rodriguez, Separation Science and Technology 45 (2010) 1595–1602.
[14] C. Catrinescu, D. Arsene, C. Teodosiu, Applied Catalysis B 101 (2011) 451–460.
[15] J.A. Zazo, J.A. Casas, A.F. Mohedano, J.J. Rodriguez, Applied Catalysis B 65 (2006) 261–268.
[16] A. Rey, M. Faraldos, J.A. Casas, J.A. Zazo, A. Bahamonde, J.J. Rodriguez, Applied Catalysis B 86 (2009) 69–77.
[17] S. Navalon, M. Alvaro, H. Garcia, Applied Catalysis B 99 (2010) 1–26.
[18] P. Bautista, A.F. Mohedano, N. Menéndez, J.A. Casas, J.J. Rodriguez, Catalysis Today 151 (2010) 148–152.
[19] P. Bautista, A.F. Mohedano, N. Menéndez, J.A. Casas, J.A. Zazo, J.J. Rodriguez, Journal of Chemical Technology and Biotechnology 86 (2011) 497–504.
[20] W.P. Kwan, B.M. Voelker, Environmental Science and Technology 37 (2003) 1150–1158.
[21] L. Xu, J. Wang, Applied Catalysis B 123–124 (2012) 117–126.
[22] L. Zhang, G.C. Papaefthymiou, J.Y. Ying, Journal of Physical Chemistry 105 (2001) 7414–7423.
[23] T.D. Nguyen, N.H. Phan, M.H. Do, K.T. Ngo, Journal of Hazardous Materials 185 (2011) 653–661.
[24] L. Xu, J. Wang, Environmental Science & Technology 46 (2012) 10145–10153.
[25] J. Lee, S. Jin, Y. Hwang, J.G. Park, H.M. Park, T. Hyeon, Carbon 43 (2005) 2536–2543.
[26] R.A. Brand, Nuclear Instruments and Methods in Physics Research B28 (1987) 398–416.
[27] J.J. Pignatello, E. Oliveros, A. Mackay, Critical Reviews in Environmental Science and Technology 36 (2006) 1–84.
[28] M. Sievers, Treatise Water Science 4 (2011) 377–408.
[29] G. Pliego, J.A. Zazo, S. Blasco, J.A. Casas, J.J. Rodriguez, Industrial & Engineering Chemistry Research 51 (2012) 2888–3896.
[30] P. Lampi, T. Vartiainen, J. Toumisto, A. Hesso, Chemosphere 20 (1990) 625–634.
[31] M.Y. Ghaly, G. Härtel, R. Mayer, R. Haseneder, Waste Management 21 (2001) 41–47.
[32] J. Qin, Q. Zhang, K.T. Chuang, Applied Catalysis B 29 (2001) 115–123.
[33] M. Munoz, Z.M. de Pedro, J.A. Casas, J.J. Rodriguez, Journal of Hazardous Materials 190 (2011) 993–1000.
[34] M. Munoz, Z.M. de Pedro, G. Pliego, J.A. Casas, J.J. Rodriguez, Industrial & Engineering Chemistry Research 51 (2012) 13092–13099.
[35] G.M. Eisenberg, Industrial & Engineering Chemistry Research 15 (1943) 327–328.
[36] E.B. Sandell, Colorimetric Determination of Traces of Metals, Interscience Pubs., New York, 1959.
[37] W. Kündig, H. Bömmel, G. Constabaris, R.H. Lidquist, Physical Review 142 (1966) 327–333.
[38] N.N. Greenwood, T.C. Gibb, Mössbauer Spectroscopy, Chapman and Hall, London, 1971.
[39] T. Yamashita, P. Hayes, Applied Surface Science 254 (2008) 2441–2449.
[40] M. Descostes, F. Mercier, N. Thromat, C. Beaucaire, M. Gautier-Soyer, Applied Surface Science 165 (2000) 288–302.
[41] Y. Ao, J. Xu, D. Fu, X. Shen, C. Yuan, Separation and Purification Technology 61 (2008) 436–441.
[42] A. Rey, D.H. Quiñones, P.M. Álvarez, F.J. Beltrán, P.K. Plicinski, Applied Catalysis B 111–112 (2012) 246–253.
[43] W.Z. Tang, C.P. Huang, Chemosphere 33 (1996) 1621–1635.
[44] C.P. Huang, C. Dong, Z. Tang, Waste Management 13 (1993) 361–377.
[45] C. Catrinescu, D. Arsene, P. Apopei, C. Teodosiu, Applied Clay Science 58 (2012) 96–101.